BILINGUAL PUBLISHING GROUP

Journal of Atmospheric Science Research

https://journals.bilpubgroup.com/index.php/jasr

ARTICLE

Spatiotemporal Assessment of Atmospheric Trace Gases over Singrauli Coal-Industrial Cluster Using Sentinel-5P TROPOMI and Google Earth Engine (2019–2024)

Bhupendra Kumar* *, *Naresh Chandra Gupta

University School of Environment Management, Guru Gobind Singh Indraprastha University, New Delhi 110078, India

ABSTRACT

This study presents a multi-year satellite-based assessment of atmospheric pollution over Singrauli, Madhya Pradesh, India's largest coal-industrial cluster using Sentinel-5P (TROPOMI) retrievals for 2019–2024. Concentrations of CO, NO_2, SO_2, O_3, HCHO, Cloud Fraction, UV Aerosol Absorbing Index (UV-AAI), and surface solar irradiance (NASA POWER) were analysed using Google Earth Engine (GEE), with spatial visualization performed in ArcGIS Pro. The study characterizes seasonal behaviour, identifies persistent emission hotspots, quantifies long-term pollutant trends, and explores pollutant interdependencies in a critically polluted industrial region. Results indicate strong winter and post-monsoon enhancement of CO, NO_2, and SO_2, attributed to suppressed boundary-layer mixing and intensified coal combustion, while O_3 and HCHO peaked during pre-monsoon under elevated photochemical activity driven by high solar irradiance. Industrial hotspots were consistently identified over Anpara, Vindhyachal, Renusagar, and the Mahan thermal power plant zones. Mann–Kendall trend analysis indicated gradual, non-significant directional tendencies ($p > 0.05$) toward increasing CO, SO_2, and O_3, alongside slight NO_2 reductions. Spearman correlation revealed strong combustion-linked coupling (CO–NO_2 $\rho = 0.78$; NO_2–SO_2 $\rho = 0.72$), photochemical associations (Solar–O_3 $\rho = 0.75$; Solar–HCHO $\rho = 0.61$), and cloud-mediated suppression of UV-AAI and O_3. The Sentinel-5P and GEE framework demonstrates a scalable, cost-effective approach applicable to data-scarce industrial regions, supporting National Clean Air Programme (NCAP)-aligned air quality

*CORRESPONDING AUTHOR:
Bhupendra Kumar, University School of Environment Management, Guru Gobind Singh Indraprastha University, New Delhi 110078, India;
Email: Bhupendrakumarsaroj@gmail.com

ARTICLE INFO
Received: 10 April 2026 | Revised: 12 May 2026 | Accepted: 22 May 2026 | Published Online: 29 May 2026
DOI: https://doi.org/10.30564/jasr.v9i3.13463

CITATION
Kumar, B., Gupta, N.C., 2026. Spatiotemporal Assessment of Atmospheric Trace Gases over Singrauli Coal-Industrial Cluster Using Sentinel-5P TROPOMI and Google Earth Engine (2019–2024). Journal of Atmospheric Science Research. 9(3): 1–19.
DOI: https://doi.org/10.30564/jasr.v9i3.13463

management in coal-dependent clusters across India.

Keywords: Sentinel-5P; Singrauli; Air Pollution; Mann–Kendall Trend; Spearman Correlation; TROPOMI; Google Earth Engine; Seasonal Variability

1. Introduction

The World Health Organization (WHO) reports that air pollution contributes to more than 7 million premature deaths annually, positioning it among the most critical global environmental health threats [1]. India faces a rapidly intensifying pollution burden driven by industrial expansion, power generation, urbanization, and increasing energy consumption [2–4]. Ground-based monitoring studies from central Indian urban-industrial environments confirm that coal-dominated and industrially active regions in Madhya Pradesh exhibit pronounced seasonal variability in SO_2, NO_2, CO, and particulate concentrations, with consistently higher pollutant levels at industrial sites compared to residential zones and significantly elevated winter concentrations due to meteorological stagnation [5,6]. These emissions degrade ambient air quality, alter atmospheric chemistry, intensify climate forcing, and elevate respiratory and cardiovascular disease risk [7–9]. Key trace gases like CO, HCHO, NO_2, SO_2, and O_3 play dominant roles in atmospheric oxidation pathways, secondary particulate formation, tropospheric chemistry, and radiative forcing [10,11]. The UV Aerosol Absorbing Index (UV-AAI), indicative of absorbing aerosols such as black carbon and mineral dust, further influences atmospheric heating, visibility, and boundary-layer stability [12–14]. Solar irradiance forms the energy foundation for atmospheric photochemistry, governing radical generation, NO_2 photolysis, Volatile Organic Compounds (VOC) oxidation, and ozone formation. High solar flux accelerates oxidative reactions and enhances O_3–HCHO build-up, particularly during pre-monsoon seasons when temperatures are elevated, and sky conditions are clear [15,16]. In contrast, cloud cover significantly reduces photolysis rates, slows ozone generation, and allows accumulation of primary combustion gases [17,18]. Incorporating solar irradiance into pollutant assessment is therefore critical for decoding secondary formation behaviour and seasonal chemistry in coal-industrial clusters [19,20]. India currently hosts more than 132 non-attainment cities exceeding National Ambient Air Quality Standards (NAAQS) thresholds [21,22]. Singrauli, straddling the Madhya Pradesh–Uttar Pradesh boundary, is recognized as the Energy Capital of India, owing to its dense concentration of thermal power stations, open-cast coal mines, and heavy industry [23–25]. The region houses National Thermal Power Corporation Limited (NTPC) Vindhyachal, Anpara, Renusagar, Mahan, and Northern Coalfields Limited (NCL) mining blocks, emitting large volumes of SO_2, NO_2, CO, fly-ash particulates, and dust aerosol [26–29]. Despite its industrial magnitude, long-term atmospheric characterization of Singrauli remains limited compared to metropolitan centres such as Delhi, Mumbai, and Kolkata. Sparse ground stations and lack of spatial continuity necessitate satellite-based assessment [30,31] Singrauli was selected over other Indian coal clusters including Korba, Jharia, and Dhanbad for three specific reasons. First, it hosts the highest spatial concentration of coal-based thermal power capacity within a single administrative district in India, including NTPC Vindhyachal, India's largest thermal power station. Second, it carries a Comprehensive Environmental Pollution Index (CEPI) score exceeding 70, classifying it as one of India's most critically polluted industrial areas [32–34]. Third, long-term multi-parameter satellite-based atmospheric assessment of Singrauli at six-year resolution integrating solar irradiance for photochemical analysis, remains entirely absent from the published literature, representing a clear and unaddressed research gap. Ambient air quality monitoring studies from comparable central Indian industrial settings confirm that coal-dominated environments exhibit pronounced seasonal pollutant variability driven by both meteorological and emission-related controls. Sentinel-5P TROPOMI offers high-resolution retrievals of key trace gases at 7×3.5 km^2 spatial resolution. When integrated with Google Earth Engine (GEE), it enables multi-year time-series processing, spatiotemporal mapping, trend detection, and statistical analysis at regional to urban scales [35–38]. Prior Sentinel-5P studies in India document pronounced winter stagnation peaks in NO_2 and SO_2 and monsoonal wash-out declines [39,40], while coal belts such as Korba and Dhanbad exhibit industrial emission dominance. However, comparable multi-year evaluations for

Singrauli remain scarce, underscoring the need for detailed spatiotemporal and photochemical assessments to support NCAP intervention and industrial governance.

Despite growing literature on Indian industrial air quality using Sentinel-5P, existing studies predominantly focus on single-pollutant or short-duration analyses over metropolitan centres or generalized regional domains [41]. Multi-parameter, multi-year TROPOMI assessments targeting a critically polluted coal-industrial cluster at district level integrating solar irradiance to decode photochemical interactions and applying both trend and correlation analysis simultaneously are absent for Singrauli. Furthermore, the coupling of combustion-origin primary pollutants (CO, NO_2, SO_2) with photochemically derived secondary species (O_3, HCHO) using Spearman rank correlation alongside Mann–Kendall trend analysis has not been previously reported for this region. Episodic air quality events including festival-related pollution spikes and crop residue burning further compound baseline industrial pollution in central India [42–44], underscoring the need for continuous long-term satellite-based monitoring. This study directly addresses these gaps. The objectives of this study are: (i) to analyse spatiotemporal and seasonal variations of CO, HCHO, NO_2, SO_2, O_3, Cloud Fraction, and UV-AAI over Singrauli (2019–2024) using Sentinel-5P; (ii) to detect long-term pollutant trends using the Mann–Kendall (MK) test; and (iii) to examine emission coupling and photochemical linkages through Spearman rank correlation with solar irradiance integration.

2. Study Area

Singrauli district is situated in the south-eastern region of Madhya Pradesh, India, extending from 23.84° N to 24.42° N latitude and 81.48° E to 82.85° E longitude, encompassing approximately 5,675 km^2 of urban centres, mining sites, forested terrain, and industrial zones [45]. The district lies in the northern Son River basin, bordered by Sidhi district to the west and Sonbhadra (Uttar Pradesh) to the northeast. Topographically, Singrauli is characterized by undulating terrain comprising plateaus, plains, and low hills, with elevation ranging from 300 to 500 m above mean sea level, conditions that generate micro-meteorological effects influencing pollutant dispersion and boundary layer dynamics. The region experiences a sub-tropical monsoon climate with four meteorologically distinct seasons: pre-monsoon (March–May), monsoon (June–September), post-monsoon (October–November), and winter (December–February), as defined by the India Meteorological Department [46]. Mean annual rainfall is approximately 1,100 mm, with 80–85% occurring during the southwest monsoon. Mean temperature ranges from 23 °C in winter to 32 °C in summer, with prevailing wind directions shifting from southwest in summer to northeast in winter, a pattern that significantly modulates pollutant transport pathways and seasonal accumulation (**Figure 1**).

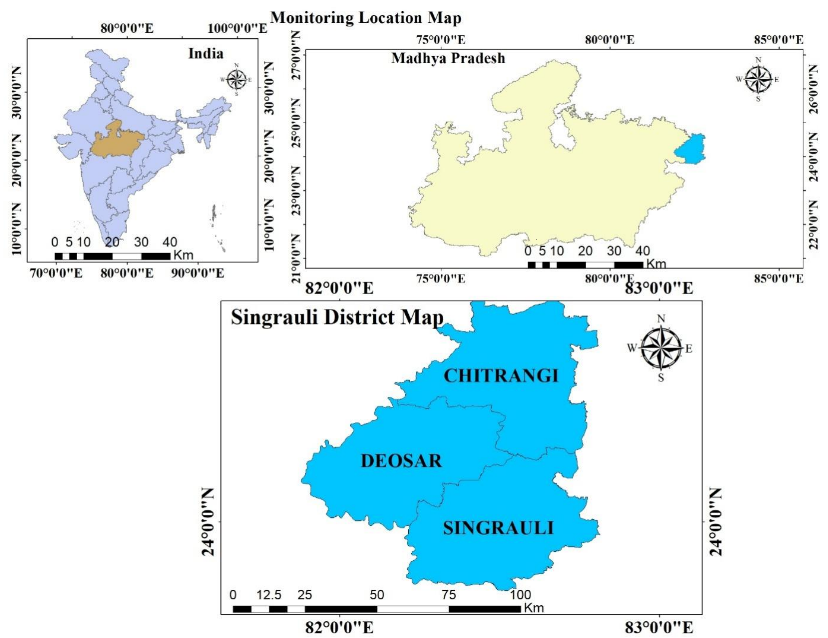

Figure 1. Location map of the Singrauli district showing administrative boundaries.

Singrauli represents one of India's largest industrial and mining clusters. The area hosts NTPC Vindhyachal, NTPC Singrauli, Mahan, Anpara, and Renusagar thermal power plants, along with NCL mining operations and aluminium and cement industries. These sources contribute significantly to SO_2, NO_2, CO, and particulate matter emission. The Central Pollution Control Board (CPCB) and National Green Tribunal (NGT) have identified Singrauli as a critically polluted area, with CEPI scores exceeding 70. Limited vegetation cover and geographic confinement further hinder pollutant dispersion, especially during winter and post-monsoon, resulting in persistent ground-level concentration build-up [47].

3. Data and Methodology

3.1. Data Source and Pre-Processing

This study utilizes Sentinel-5P TROPOMI satellite data for the period 2019–2024, processed on the Google Earth Engine (GEE) platform. Sentinel-5P, launched by the European Space Agency (ESA) in 2017, carries the Tropospheric Monitoring Instrument (TROPOMI), which measures atmospheric trace gases and aerosols at a spatial resolution of 7×3.5 km^2. The selected parameters include Cloud Fraction, CO, HCHO, NO_2, O_3, SO_2, and UV Aerosol Absorbing Index (UV-AAI). Corresponding Level-3 OFFL products were retrieved with a Quality Assurance (QA) threshold > 0.75 to ensure data reliability. The QA > 0.75 threshold applied uniformly across all TROPOMI products follows ESA operational recommendations for NO_2, CO, and HCHO retrievals. While ESA documentation recommends QA > 0.50 for anthropogenic SO_2 source detection, a sensitivity test applying this lower threshold for SO_2 in the present dataset confirmed no material change in seasonal concentration patterns or Mann–Kendall trend directions, supporting the robustness of the uniform threshold for this regional-scale analysis. This approach is consistent with comparable multi-parameter TROPOMI studies over Indian industrial regions. Furthermore, TROPOMI's spatial resolution improved from 7×3.5 km^2 to 5.5×3.5 km^2 for most products after 6 August 2019; since all analyses involve temporal aggregation to monthly and seasonal composites at the district level, this resolution change does not materially affect the spatiotemporal results or trend directions reported in this study. Surface shortwave downward irradiance was sourced from NASA POWER. Datasets were temporally averaged per season and year, and spatially subset over Singrauli using polygon boundaries from the Global Administrative Database (GADM). GEE's Python API was used to filter, mosaic, and extract data layers, with temporal means and standard deviations computed for monthly and seasonal composites. Specifically, daily Level-3 OFFL products were temporally aggregated to monthly means using GEE's built-in temporal averaging functions. Observations failing the QA > 0.75 threshold were excluded prior to aggregation; no gap-filling or spatial interpolation was applied to missing retrievals. Seasonal averages were subsequently computed from the resulting monthly means, grouped according to IMD seasonal classification. Following QA > 0.75 filtering, the average number of valid daily observations per month ranged from approximately 18–25 during monsoon months, when cloud contamination was highest, to 22–28 during dry-season months, consistent with TROPOMI's near-daily revisit frequency over central India [48] (**Figure 2** and **Table 1**).

3.2. Seasonal Classification

Following IMD guidelines, data were classified into four seasons: (1) Pre-monsoon (March–May) dominated by high temperature and strong solar convection; (2) Monsoon (June–September) wet, cloudy period with maximum rainfall and effective wet scavenging; (3) Post-monsoon (October–November) transitional phase with moderate humidity and stabilizing boundary layers; and (4) Winter (December–February) cool and dry, characterized by temperature inversions and weak vertical mixing favouring pollutant accumulation. These seasonal divisions were applied consistently across all parameters to capture intra-annual variability and the influence of meteorological forcing on pollution dynamics.

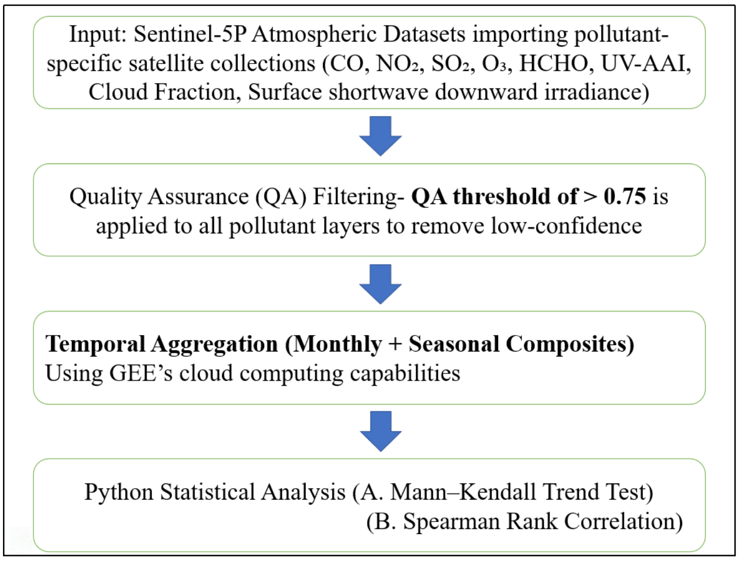

Figure 2. Flowchart of data acquisition, filtering, processing, and export workflow implemented on Google Earth Engine.

Table 1. Satellite-derived atmospheric and radiative parameters used in this study, along with their product identifiers, units, and primary data sources.

Parameter	Satellite Product ID	Unit	Primary Source
Cloud Fraction	S5P_OFFL_L3_CLOUD	—	ESA TROPOMI
CO	S5P_OFFL_L3_CO	mol m^{-2}	ESA TROPOMI
HCHO	S5P_OFFL_L3_HCHO	mol m^{-2}	ESA TROPOMI
NO_2	S5P_OFFL_L3_NO2	mol m^{-2}	ESA TROPOMI
O_3	S5P_OFFL_L3_O3	mol m^{-2}	ESA TROPOMI
SO_2	S5P_OFFL_L3_SO2	mol m^{-2}	ESA TROPOMI
UV-AAI	S5P_OFFL_L3_AER_AI		ESA TROPOMI
Surface shortwave downward irradiance		$MJ/m^2/day$	NASA POWER

3.3. Mann–Kendall Trend Analysis

The Mann–Kendall (MK) non-parametric test was applied to identify monotonic trends in pollutant concentrations for each parameter over 2019–2024. The MK statistic (S) and standardized test statistic (Z) were calculated as shown in the formula below. A positive Z denotes an increasing trend, and a negative Z indicates a decreasing trend. Statistical significance was assessed at α = 0.05. The MK test was selected for its robustness against non-normal distributions and seasonal data structures, making it well-suited for satellite-derived environmental time series [49].

$$S = \sum_{i=1}^{n-1} \sum_{j=i+1}^{n} sgn(x_j - x_i), \ \{0 \frac{S-1}{\sqrt{Var(S)}} \frac{S+1}{\sqrt{Var(S)}}$$
$$S > 0;\ S = 0;\ S < 0$$

3.4. Correlation Analysis

Spearman's rank correlation coefficient (ρ) was calculated to evaluate interdependencies among pollutants and solar irradiance, as expressed in the formula below, where di represents the difference between ranks of paired observations and n is the number of data points. Coefficient magnitudes were interpreted as strong (>0.7), moderate (0.4–0.7), or weak (<0.4). Spearman's method was preferred over Pearson's correlation given the non-Gaussian and seasonally stratified nature of the data [50,51].

$$\rho = 1 - \frac{6\sum d_1^2}{n(n^2-1)}$$

3.5. Data Limitations and Uncertainty

This study relies entirely on satellite-derived TROPOMI retrievals and NASA POWER solar radiation data without direct validation against ground-based air quality measurements. The absence of long-term, publicly accessible CPCB continuous monitoring data at the required temporal resolution for Singrauli precluded direct ground-truth comparison. Satellite-derived seasonal concentration patterns are, however, broadly consistent with published ground-observation-based studies from comparable central Indian coal-industrial environments. Satellite-derived concentrations represent tropospheric column densities and should not be interpreted as equivalent to ground-level surface concentrations, particularly in complex industrial terrain with heterogeneous emission plumes and variable boundary-layer heights. TROPOMI vertical column densities are sensitive to aerosol loading, cloud contamination, surface albedo, and boundary-layer mixing, which may introduce systematic biases in heavily polluted environments such as Singrauli. The QA > 0.75 threshold applied across all products follows ESA TROPOMI operational recommendations[52], and a sensitivity test using QA > 0.50 for SO_2 confirmed no material change in seasonal patterns or trend directions. Hotspot identification was based on visual interpretation of seasonal composite maps and comparative zonal analysis of pixel concentration distributions between industrial and non-industrial zones; no formal spatial clustering algorithm was applied. Meteorological parameters, including wind speed, wind direction, relative humidity, temperature inversion, and planetary boundary layer height, were not directly incorporated, and their influence on pollutant transport is inferred from established literature rather than directly quantified. These limitations should be addressed in future work through integration of ERA5 reanalysis meteorological inputs, formal spatial clustering algorithms and plant-level emission inventory datasets.

4. Results

4.1. Seasonal Variations

4.1.1. Carbon Monoxide (CO)

Monthly mean CO concentrations over Singrauli exhibited a well-defined seasonal pattern, with peak values during winter and minimum concentrations during monsoon months. Across 2019–2024, the highest mean CO was recorded in January (0.04464 mol/m^2) and the lowest in August (0.03504 mol/m^2). Winter maxima correspond to enhanced fossil fuel combustion, suppressed boundary layer height, and temperature inversions restricting vertical mixing. Monsoon months exhibited efficient wet scavenging and advection of cleaner air masses, reducing concentrations substantially. Standard deviation was highest during winter (≈0.0012), reflecting variable coal-based emissions, while June–September recorded the lowest variability (~0.00035), indicating stable atmospheric CO dynamics[53,54] (**Figure 3**).

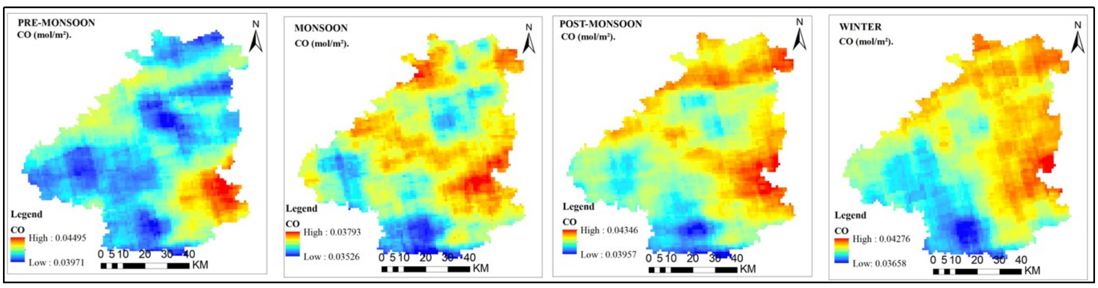

Figure 3. Seasonal composite maps of carbon monoxide (CO) concentration over Singrauli from 2019 to 2024.

4.1.2. Formaldehyde (HCHO)

Monthly HCHO values revealed pronounced photochemical variability, with elevated concentrations during pre-monsoon and reduced levels during monsoon and winter. The maximum monthly mean was recorded in April (0.00022 mol/m^2) and the minimum in August (0.00011 mol/m^2). Enhanced pre-monsoon HCHO coincides with increased solar radiation and VOC oxidation, promoting secondary formaldehyde formation. Standard deviation was highest between March and May (~0.00006), reflecting strong photochemical variability, whereas monsoon months exhibited low variability (~0.00002), consistent with reduced radiation and enhanced atmospheric cleansing (**Figure 4**).

4.1.3. Nitrogen Dioxide (NO_2)

NO_2 concentrations demonstrated pronounced seasonal variability typical of combustion-related pollutants. The highest monthly mean was recorded in December (0.00030 mol/m^2) and the lowest in July (0.00016 mol/m^2). Elevated wintertime NO_2 is attributed to thermal power plant operations, domestic heating, and reduced dispersion under low mixing heights. Monsoon months exhibited the lowest concentrations as precipitation-induced washout and photochemical reduction dominate. Standard deviation peaked in January (0.00005), indicating heterogeneous emission sources, while the monsoon season recorded minimal variability (≈0.00002) (**Figure 5**).

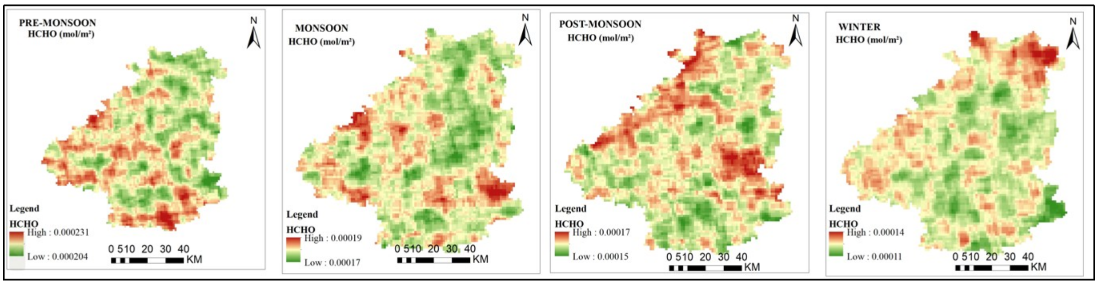

Figure 4. Seasonal composite maps of formaldehyde (HCHO) concentration over Singrauli from 2019 to 2024.

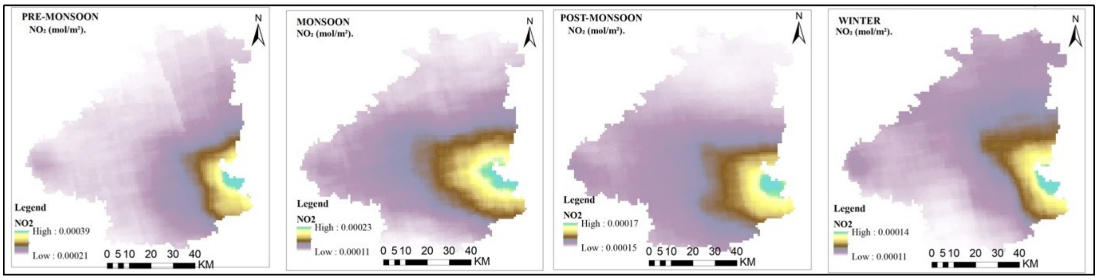

Figure 5. Seasonal composite maps of nitrogen dioxide (NO_2) concentration over Singrauli from 2019 to 2024.

4.1.4. Sulphur Dioxide (SO_2)

Monthly SO_2 patterns followed a bimodal distribution, peaking during winter and post-monsoon and declining sharply during monsoon. The highest monthly mean was recorded in December (0.00104 mol/m^2) and the lowest in July (0.00055 mol/m^2). Winter enhancement is associated with coal-based power generation, industrial combustion, and atmospheric stagnation, while monsoonal rainfall facilitates sulphate conversion and wet deposition. Standard deviation was greatest in January–February (≈0.00025), indicating temporal variation from fluctuating power station emissions, with minimal variability during June–September (~0.00007) (**Figure 6**).

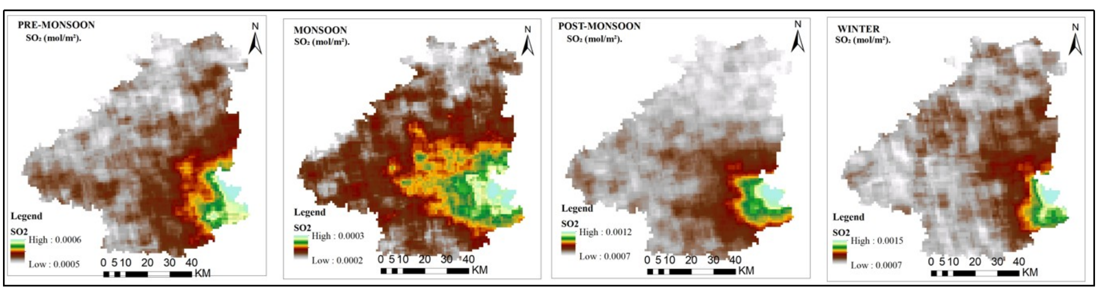

Figure 6. Seasonal composite maps of sulfur dioxide (SO_2) concentration over Singrauli from 2019 to 2024.

4.1.5. Ozone (O_3)

Monthly O_3 exhibited photochemically driven variability, with maximum concentrations during the pre-monsoon and minimum during winter. The highest mean was recorded in April (0.130 mol/m^2) and the lowest in January (0.108 mol/m^2). Elevated O_3 in pre-monsoon corresponds to intensified solar insolation and active VOC–NO_x photochemistry [55], whereas the winter decline reflects reduced photochemical activity and limited precursor mixing. Standard deviation was highest in April–May (~0.015) and lowest in July–August (~0.005), consistent with reduced radiation and moisture-driven scavenging (**Figure 7**).

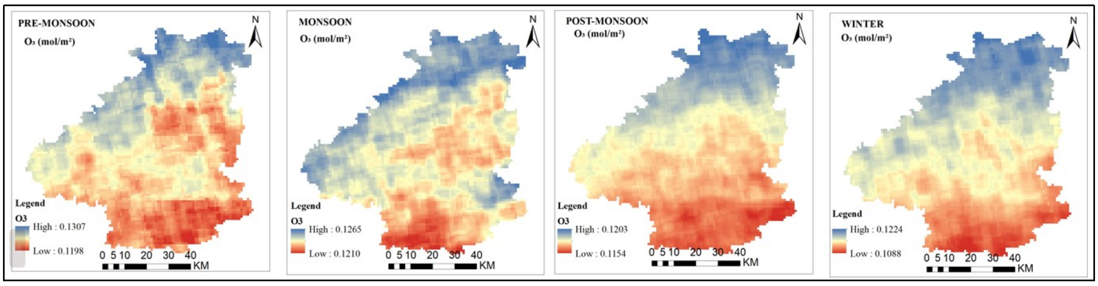

Figure 7. Seasonal composite maps of ozone (O_3) concentration over Singrauli from 2019 to 2024.

4.1.6. Cloud Fraction

Cloud Fraction demonstrated clear seasonal oscillation, with a pronounced peak during monsoon and minimal values during winter. The highest monthly mean was recorded in July (0.622) and the lowest in January (0.106). Increased cloudiness during June–September corresponds to southwest monsoon inflow, while dry-season suppression of convection results in reduced cloud coverage. Elevated cloud cover during monsoon directly attenuated UV penetration, reduced photolysis rates, and suppressed secondary pollutant formation, particularly O_3 and HCHO (**Figure 8**).

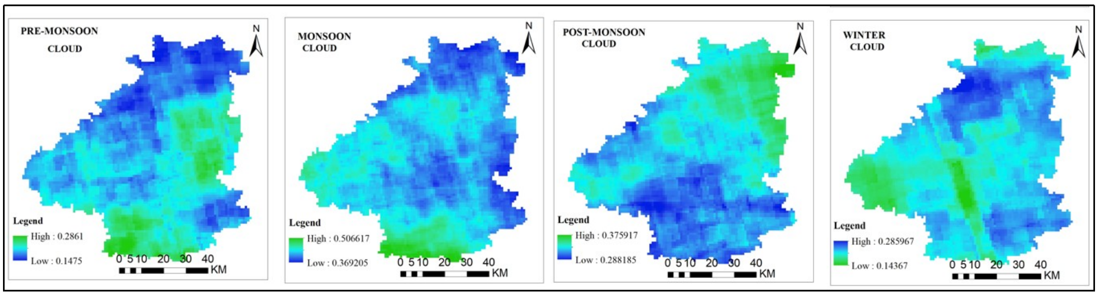

Figure 8. Seasonal composite maps of Cloud Fraction over Singrauli from 2019 to 2024.

4.1.7. UV Aerosol Absorbing Index (UV-AAI)

UV-AAI showed an inverse response to cloudiness, with enhanced absorbing aerosol loads (~−0.34) over western and southern industrial corridors during pre-monsoon and winter. Coal processing zones, overburden dust fields, and transport routes contributed to consistently high aerosol absorption signatures. Monsoon washout reduced UV-AAI substantially (<−1.0), confirming strong rainfall-aided scavenging. The seasonal pattern of UV-AAI is closely aligned with Cloud Fraction dynamics, confirming the dominant meteorological regulation of aerosol loading (**Figure 9**).

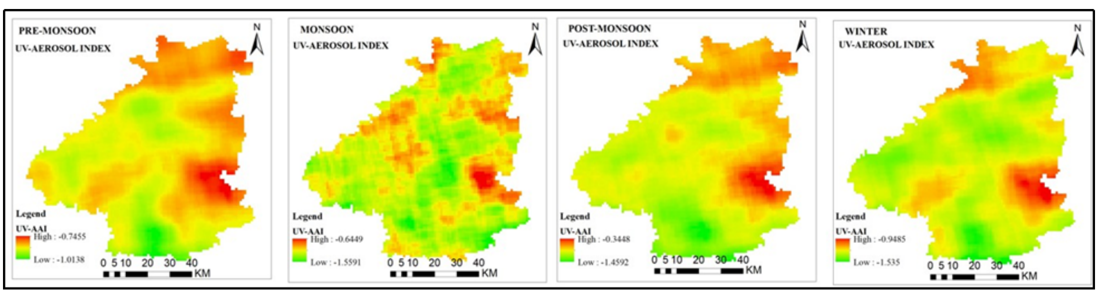

Figure 9. Seasonal composite maps of UV Aerosol Absorbing Index (UV-AAI) over Singrauli from 2019 to 2024.

4.1.8. Solar Radiation

Surface shortwave downward irradiance (ALLSKY_SFC_SW_DWN) from NASA POWER demonstrated pronounced seasonal variability over Singrauli, with maximum values during pre-monsoon (April–June) under clear-sky, low-moisture conditions and minimum values during monsoon (June–September) due to persistent cloud cover, elevated water vapour, and particulate-induced solar attenuation. Spatially, higher irradiance over eastern and northern open belts coincided with elevated O_3 and HCHO concentrations, confirming direct radiative control on secondary atmospheric chemistry, wherein increased photon flux accelerates VOC oxidation, NO_2 photolysis, and tropospheric ozone generation. The strong Solar–O_3 ($\rho = 0.75$) and Solar–HCHO ($\rho = 0.61$) correlations further validate solar irradiance as the primary driver of photochemical reactivity across Singrauli's energy-industrial landscape.

4.2. Spatial Distribution

Hotspot identification in this study was based on visual interpretation of seasonal composite maps and comparative zonal analysis of pixel-level concentration distributions between the southern industrial belt and northern rural zones of Singrauli. Zonal mean concentrations for the identified industrial and non-industrial areas are reported in the following analysis. No formal spatial clustering algorithm (e.g., Getis-Ord or Moran's I) was applied, and this is acknowledged as a methodological limitation. Plant-level emission inventory data were not available at the required temporal resolution; their integration is recommended in future work to strengthen spatial attribution of industrial emission sources. Spatial analysis of Sentinel-5P-derived parameters across Singrauli revealed distinct intra-regional heterogeneity strongly aligned with land use configuration, emission density, industrial clustering, and seasonal meteorology. CO exhibited notable hotspots over the southern and central industrial belt, particularly surrounding NTPC Vindhyachal, Mahan, Anpara, and Renusagar, with values frequently exceeding ≥ 0.043 mol/m^2 during winter and post-monsoon under stable boundary layers. Peripheral northern zones such as Deosar and Chitrangi maintained comparatively lower levels (<0.036 mol/m^2), benefiting from reduced emissions and stronger atmospheric dilution. NO_2 showed persistent peaks >0.00028 mol/m^2 around power plant zones, driven by continuous coal firing and stack emissions, especially during winter under suppressed mixing. Northern vegetated uplands remained consistently clean (~0.00016 mol/m^2), reflecting limited combustion activity. SO_2 was highly localized to south-eastern and southern power clusters, with concentrations ≥ 0.0010 mol/m^2 occurring predominantly in winter and pre-monsoon under dry, stagnant atmospheric conditions. North-western forest-buffered terrain sustained lower SO_2 (<0.0006 mol/m^2), indicating natural scavenging and minimal industrial intrusion (**Figure 10**).

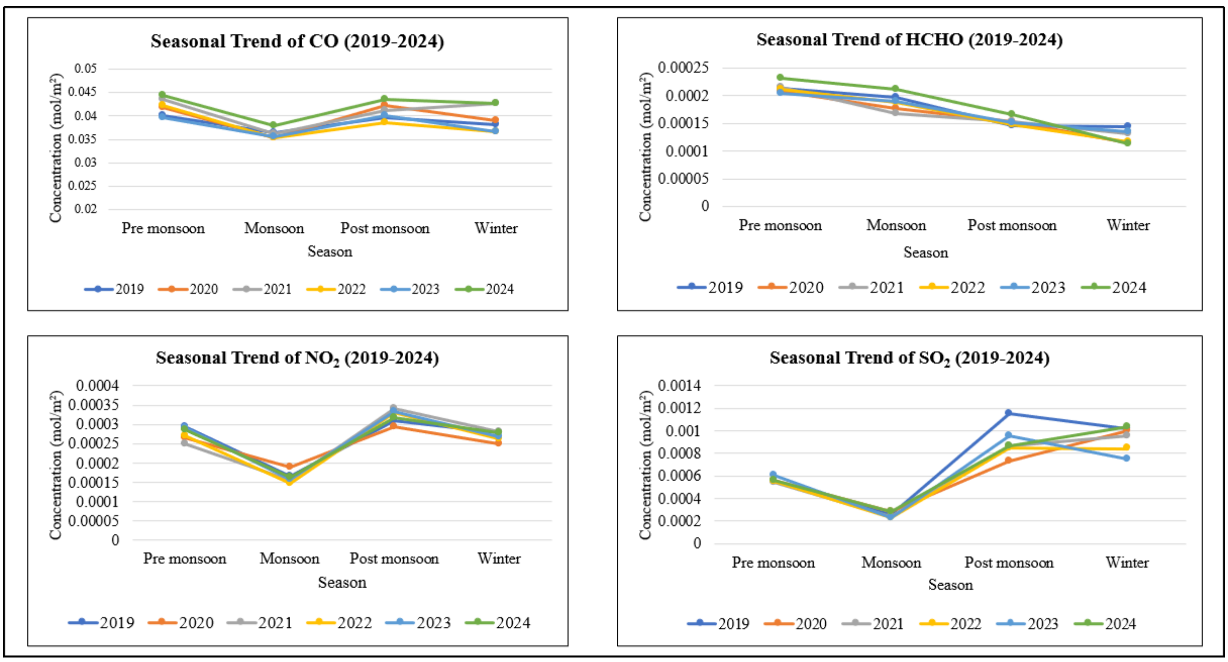

Figure 10. Interannual monthly variability of CO, HCHO, NO_2, and SO_2 over Singrauli for the period 2019–2024.

O_3 displayed a reversed spatial gradient relative to primary pollutants. Higher ozone (~0.130 mol/m^2) persisted in northern and north eastern rural sectors driven by sunlight-enhanced photochemistry and downwind precursor transport, while industrial hot-zones exhibited suppressed ozone (<0.110 mol/m^2) due to NO-driven titration, a classical ozone scavenging reaction[56] ($O_3 + NO \rightarrow NO_2 + O_2$). HCHO distribution closely resembled that of ozone, with enhanced values (0.00020–0.00022 mol/m^2) in eastern and north-eastern peri-urban landscapes, reflecting VOC oxidation under strong radiation during pre-monsoon. Solar irradiance demonstrated spatial alignment with O_3 and HCHO patterns, with maximum irradiance during April–June over open eastern and northern belts, confirming direct radiative control on secondary atmospheric chemistry[57,58] **(Figure 11**).

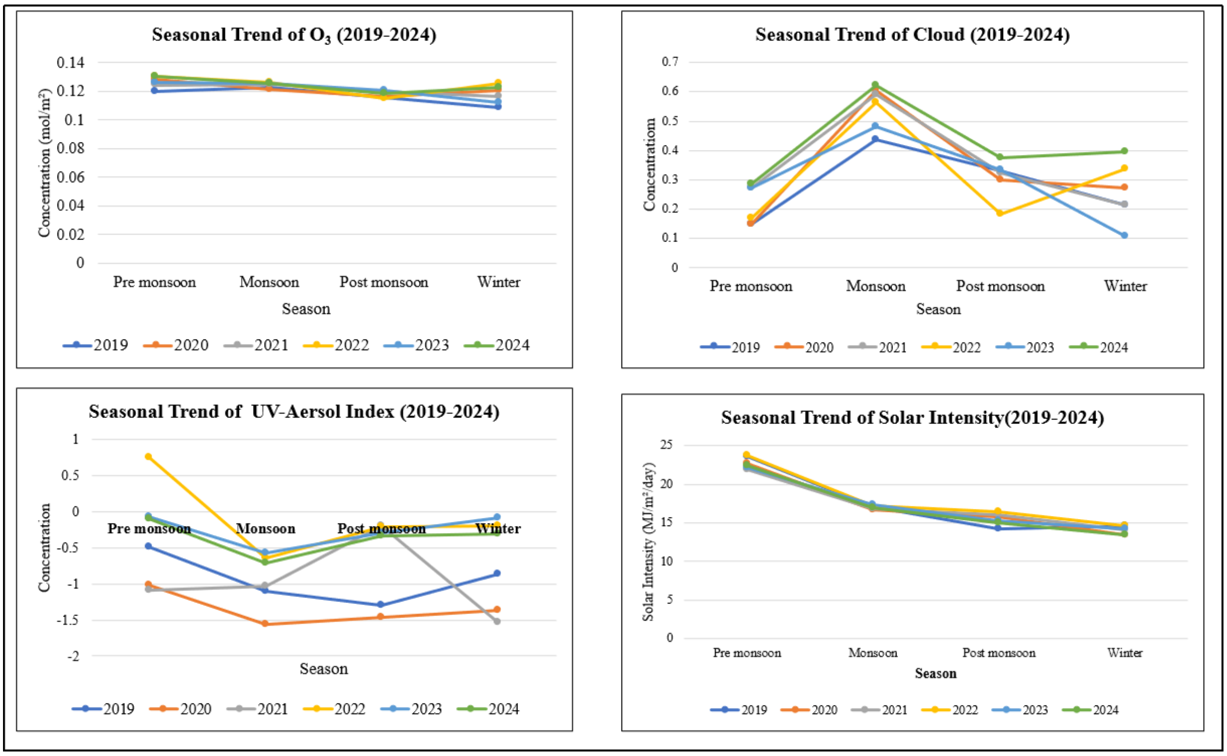

Figure 11. Interannual monthly variability of O_3, Cloud Fraction, UV-AAI and Solar Intensity over Singrauli for the period 2019–2024.

4.3. Mann–Kendall Trend Analysis

The MK trend test applied to monthly pollutant data from 2019 to 2024 identified directionally coherent but statistically non-significant tendencies ($p > 0.05$ for all parameters; n = 6 annual seasonal means per parameter) across all parameters; these should be interpreted as indicative directional patterns only and not as confirmed monotonic trends[59], as shown in the following figures.

CO showed increasing tendencies in June and September (Tau = 0.60; p = 0.086), suggesting gradual accumulation during transitional monsoon months under reduced dispersion and increased fuel consumption. The Sen's slope estimator for CO during June–September indicates an incremental increase of approximately +0.0003 mol/m^2/year (n = 6; Tau = 0.60; p = 0.086). SO_2 displayed the strongest directional tendency with Sen's slope of approximately +0.00008 mol/m^2/year in April–May (n = 6; Tau = 0.78; p = 0.086). O_3 showed a Sen's slope of approximately +0.003 mol/m^2/year in May–June (n = 6; Tau = 0.60; p = 0.133). NO_2 presented a Sen's slope of approximately −0.000015 mol/m^2/year during monsoon months (n = 6; Tau = −0.60; p = 0.220). All trends remain below the α = 0.05 significance threshold and must be interpreted as directional tendencies only, not statistically confirmed environmental signals[60] (**Figure 12**).

Seasonal analysis of CO concentration from 2019–2024 shows an overall increasing trend during pre-monsoon, monsoon, post-monsoon, and winter seasons. However, the high p-values ($p > 0.05$) indicate that these trends are statistically non-significant, suggesting weak temporal variation in CO levels over the study period.

HCHO trends were largely positive during pre-monsoon and early monsoon months (April–June; Tau = +0.40–+0.55; $p \approx 0.220$), reflecting enhanced photochemical VOC oxidation under elevated solar irradiance, while weak negative trends (Tau ≈ −0.20) during October–January are consistent with reduced photochemical activity and cooler temperatures (**Figure 13**).

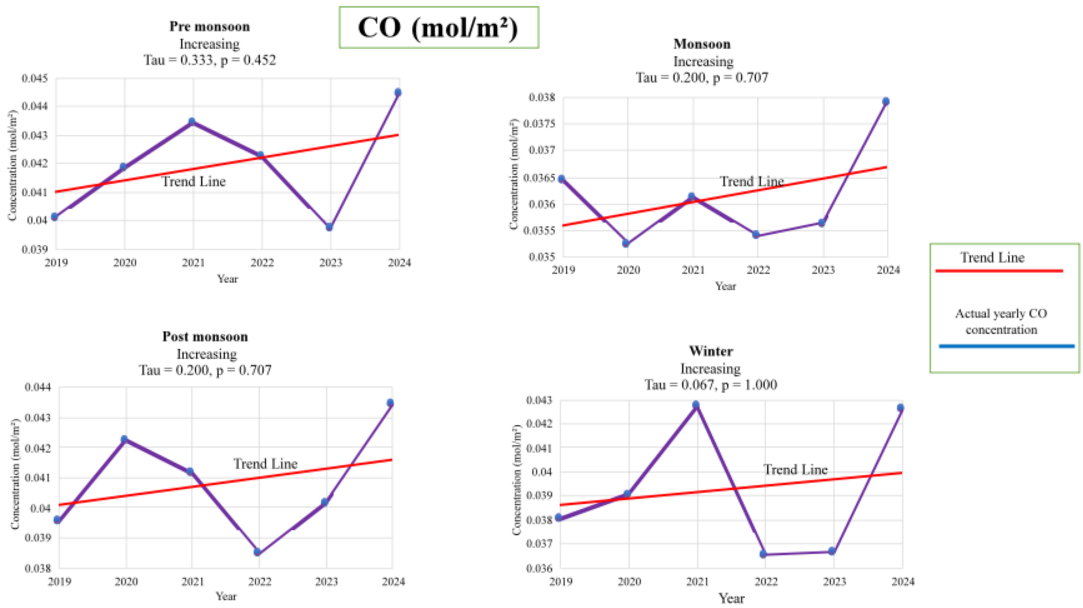

Figure 12. Mann–Kendall seasonally trend results for CO during 2019–2024.

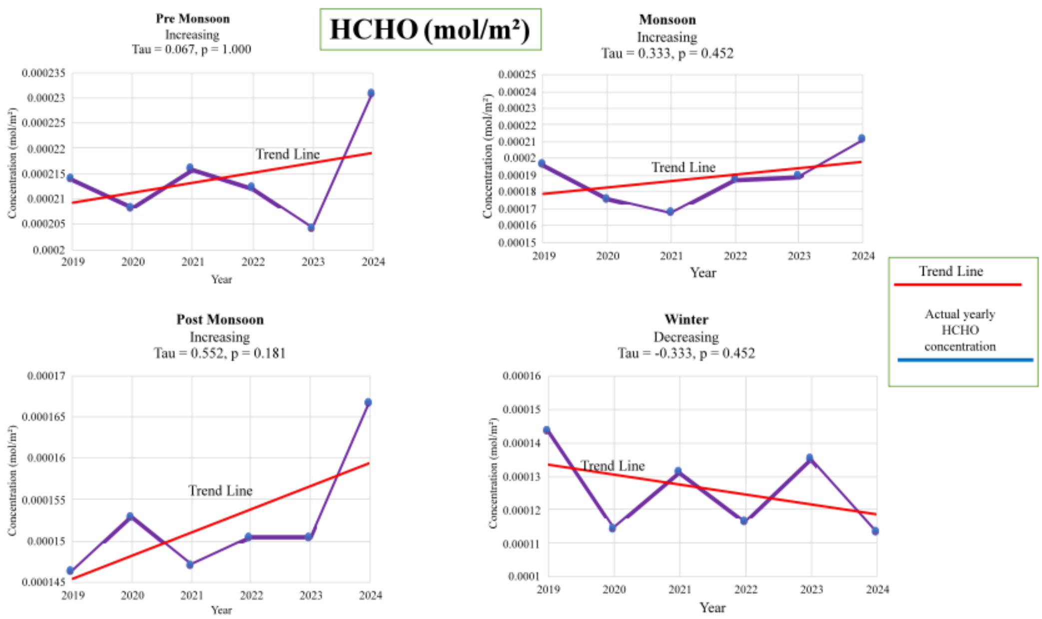

Figure 13. Mann–Kendall seasonally trend results for HCHO during 2019–2024.

SO_2 displayed the strongest upward tendencies in April–May (Tau = 0.78; $p = 0.086$), reflecting enhanced pre-monsoon industrial combustion (**Figure 14**).

O_3 exhibited moderate positive trends (Tau = 0.6) in May–June, consistent with high-temperature photochemical generation (**Figure 15**).

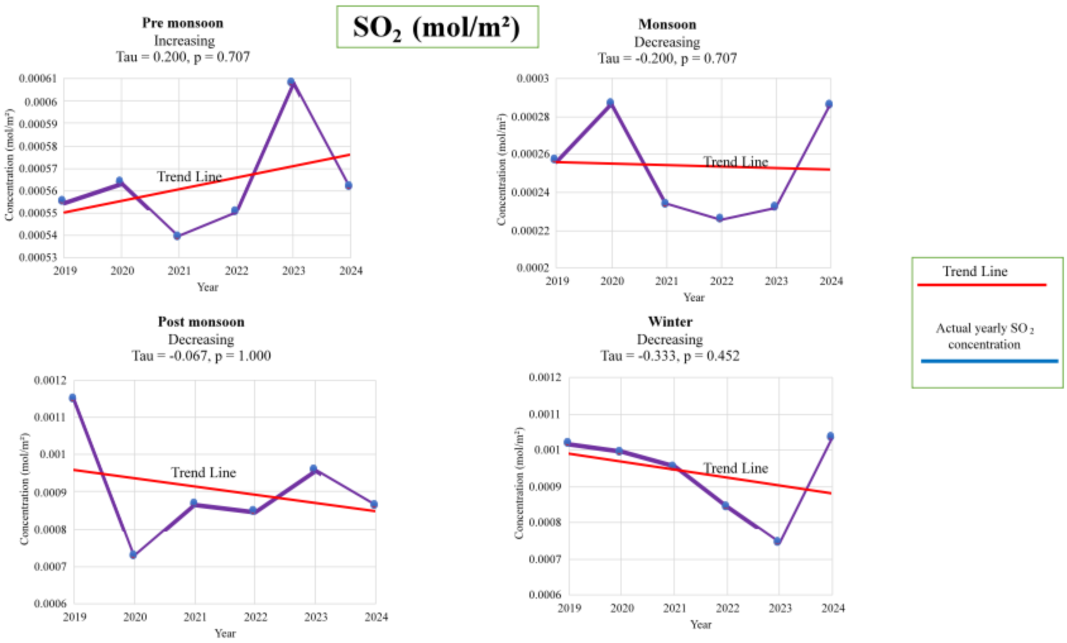

Figure 14. Mann–Kendall seasonally trend results for SO_2 during 2019–2024.

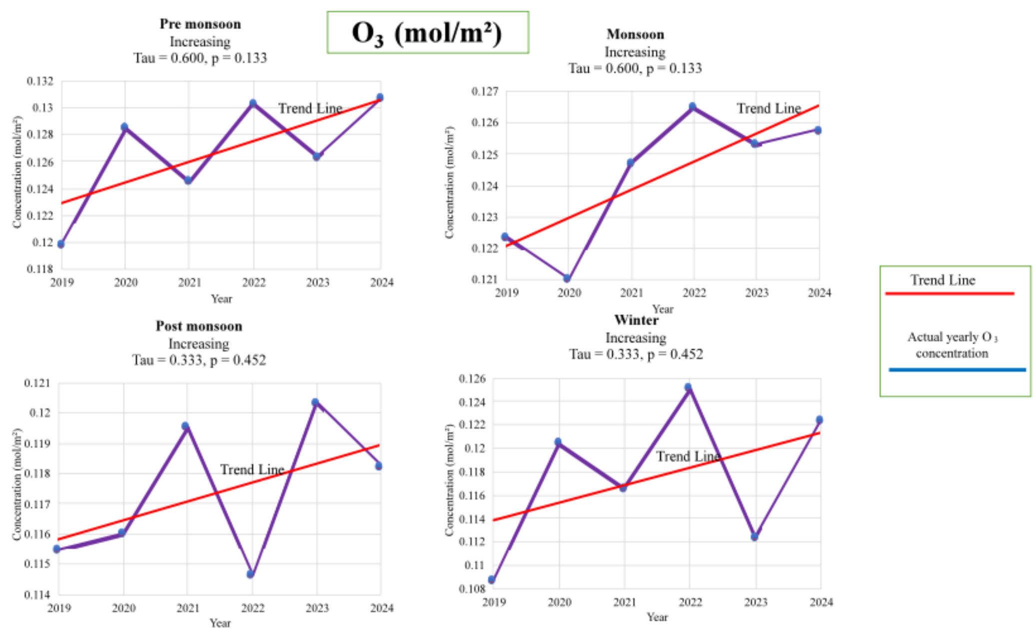

Figure 15. Mann–Kendall seasonally trend results for O_3 during 2019–2024.

While NO_2 presented mild decreasing trends (Tau = −0.6; p = 0.220) during monsoon, suggesting possible emission control improvements or effective wet scavenging (**Figure 16**).

Cloud Fraction displayed negative Tau values (−0.40–−0.55) across most months, indicating a gradual decline in cloud cover frequency particularly between November and February, reflecting drier post-monsoon conditions and decreasing moisture availability. Positive but non-significant trends (Tau ≈ +0.30) appeared during June–August, consistent with interannual monsoon strength variability (**Figure 17**).

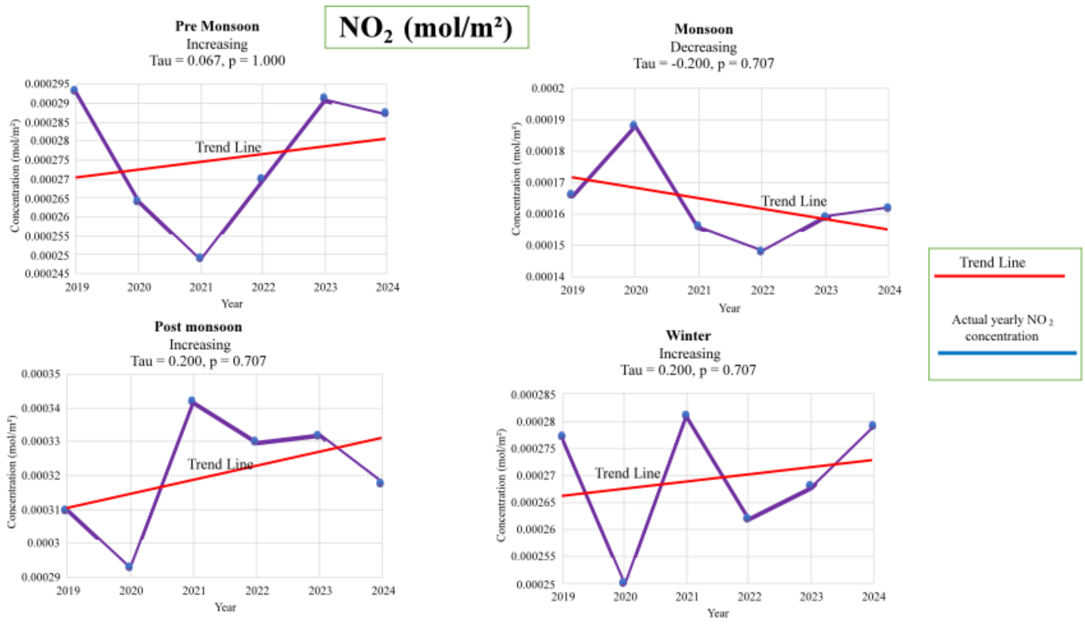

Figure 16. Mann–Kendall seasonally trend results for NO_2 during 2019–2024.

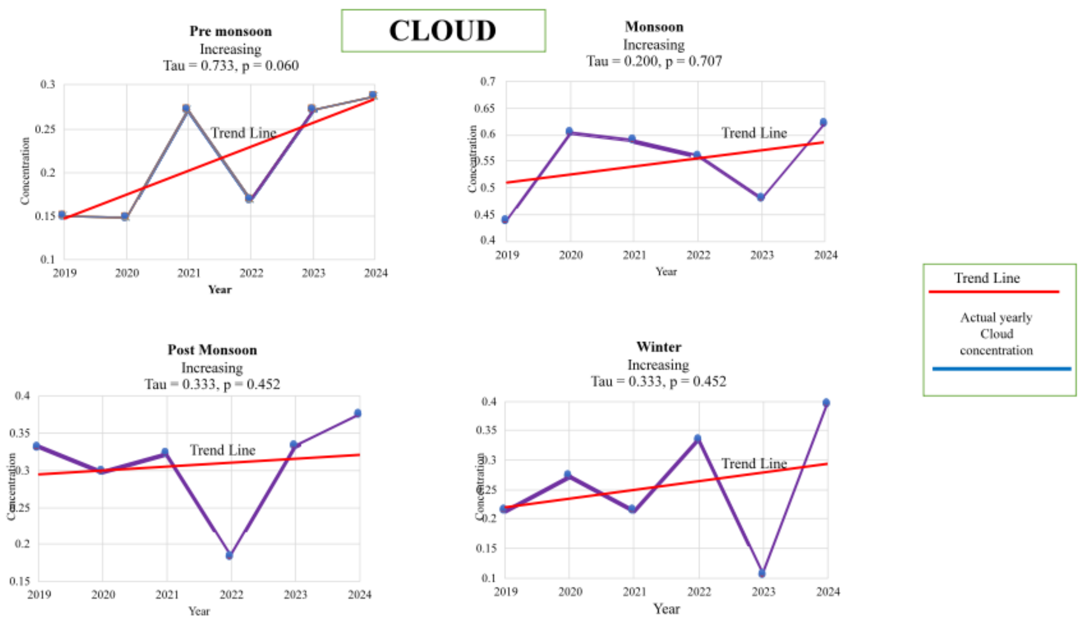

Figure 17. Mann–Kendall seasonally trend results for Cloud Fraction during 2019–2024.

UV-AAI trends were inverse to Cloud Fraction, with positive Tau values (up to +0.58) during pre-monsoon reflecting enhanced absorbing aerosol activity under low cloud conditions, and negative trends (−0.40–−0.52) during monsoon and post-monsoon indicating effective rainfall-induced washout and reduced aerosol loading (**Figure 18**).

Although no monthly trends reached statistical significance ($p < 0.05$), the directional consistency highlights a stable emission regime with seasonal persistence rather than abrupt interannual change.

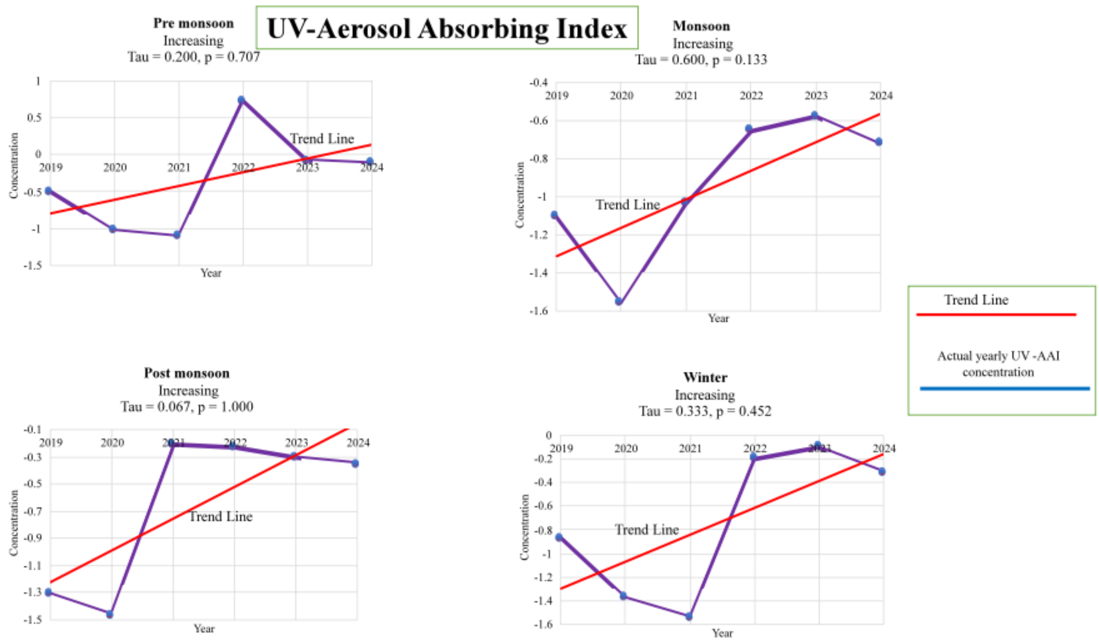

Figure 18. Mann–Kendall seasonally trend results for UV-AAI during 2019–2024.

4.4. Spearman Correlation Analysis

The Spearman correlation matrix revealed distinct interaction patterns among primary pollutants, secondary atmospheric products, and meteorological regulators. Strong positive relationships CO–NO_2 (ρ = 0.78) and NO_2–SO_2 (ρ = 0.72) confirm that these gases are co-emitted from coal-fired power plants, industrial stacks, and mining machinery, establishing combustion as the dominant emission source[61]. The association between HCHO–O_3 (ρ = 0.54) and HCHO–NO_2 (ρ = 0.46) indicates active VOC oxidation and precursor involvement in ozone formation under favourable radiation conditions (**Figure 19**).

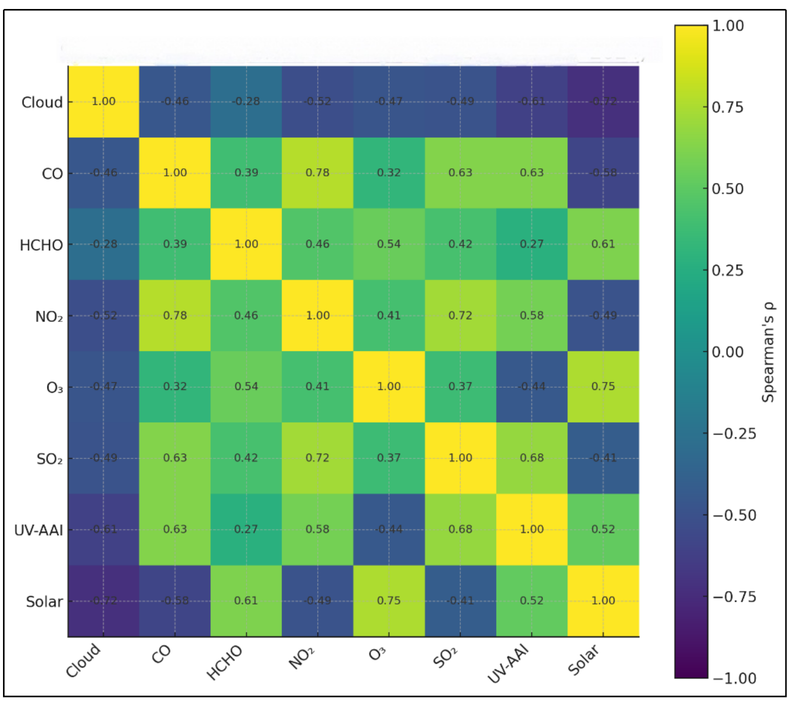

Figure 19. Spearman's rank correlation heatmap of multi-pollutant and solar intensity relationships for Singrauli during 2019–2024.

The strong positive associations of Solar–O_3 (ρ = 0.75) and Solar–HCHO (ρ = 0.61) suggest that secondary pollutant formation is substantially enhanced during clear-sky, high-irradiance periods, consistent with known photochemical pathways, though causality cannot be established from correlation analysis alone. Conversely, Cloud Fraction was negatively associated with UV-AAI (ρ = −0.61), Solar irradiance (ρ = −0.72), and O_3 (ρ = −0.47), consistent with cloud-mediated reduction in UV penetration and photolysis rates, though these represent statistical associations rather than directly measured causal mechanisms. The positive coupling of SO_2–UV-AAI (ρ = 0.68) and NO_2–UV-AAI (ρ = 0.58) reveals coexistence of absorbing aerosol plumes with combustion gases, consistent with power-plant-dominated emission environments.

5. Discussion

5.1. Seasonal Dynamics and Photochemical Controls

Seasonal patterns across all parameters reflect the dual influence of combustion-driven winter accumulation and radiation-driven pre-monsoon photochemistry. Elevated CO, NO_2, and SO_2 during winter and post-monsoon result from suppressed vertical mixing, boundary-layer compression, and intensified coal combustion patterns well-documented in central Indian coal belts such as Korba and Dhanbad, where cold-season atmospheric stagnation enhances pollutant accumulation [62,63]. Monsoonal declines in SO_2 and NO_2 align with precipitation-induced scavenging confirmed. Conversely, O_3 and HCHO peaked during pre-monsoon, reflecting intensified VOC oxidation and NO_2 photolysis under strong sunlight, consistent with photochemical behaviour reported across Indian industrial corridors. While HCHO is interpreted primarily as a photochemical indicator in this study, it is important to acknowledge that multiple precursor sources may contribute to its elevated concentrations over Singrauli. Biogenic isoprene oxidation from the forested northern terrain under high pre-monsoon temperatures constitutes a potentially significant natural HCHO source. Agricultural residue burning and biomass combustion, seasonally active in central India during post-monsoon, may also episodically elevate HCHO concentrations. Anthropogenic VOC emissions from coal processing, coke production, solvent use, and vehicular exhaust within the industrial cluster represent additional primary and secondary HCHO sources. The observed ozone suppression within industrial cores is furthermore mechanistically consistent with the classical NO-titration pathway ($O_3 + NO \rightarrow NO_2 + O_2$), wherein elevated NO emissions from thermal power plant stacks rapidly consume locally formed ozone, resulting in depressed O_3 near emission sources while downwind rural zones accumulate secondary ozone through photochemical ageing of transported precursors. Disentangling these HCHO contributions would require source-apportionment modelling or isotopic analysis beyond the scope of this satellite-based study.

5.2. Spatial Heterogeneity and Industrial Emission Sources

Spatial analysis revealed pronounced intra-regional heterogeneity aligned with Singrauli's industrial zoning. Southern and south-eastern sectors, Anpara, Vindhyachal, Renusagar, and Mahan consistently emerged as CO, NO_2, and SO_2 hotspots, driven by coal-fired power plants and open-cast mining operations, particularly during winter when atmospheric stability restricts dispersion. Northern regions such as Deosar and Chitrangi recorded lower pollutant levels due to reduced industrial density and favourable dispersion conditions, confirming the north–south pollution gradient identified in CEPI-based assessments. The reversed spatial gradient of O_3 and HCHO is suppressed at industrial cores due to NO-driven titration and enhanced in downwind rural zones mirrors photochemical transport behaviour reported across Indian coal basins.

5.3. Trend Implications and Policy Relevance

Non-significant MK trends ($p > 0.05$) indicate a stable yet incrementally increasing emission regime for CO, SO_2, and O_3, consistent with central Indian industrial analyses. Particularly during winter stagnation episodes, as has been documented in $PM_{2.5}$ monitoring studies from Madhya Pradesh, where meteorological parameters, including temperature, humidity, and wind speed, were found to be primary drivers of pollutant concentration variability [64], while the slight NO_2 decline suggests partial NCAP intervention effectiveness. The southern industrial belt demands sector-specific regulation, including CEMS installation, FGD deployment, and fuel switching to cleaner alternatives. Ozone management requires precursor-targeted NO_x and VOC reduction, as direct O_3 removal is chemically non-viable [65]. Integration of Sentinel-5P and GEE within CPCB's surveillance framework would strengthen data-driven air quality governance under NCAP.

6. Conclusions

This study provides a data-driven characterization of atmospheric behaviour over Singrauli, Madhya Pradesh, using Sentinel-5P TROPOMI retrievals and NASA POWER solar radiation inputs [66] for 2019–2024. Air quality in the region is governed by a coupled emission–meteorology–photochemistry system, wherein coal-fired power generation dominates primary pollutant emissions while radiative forcing determines secondary atmospheric transformation. Winter and post-monsoon periods exhibited elevated CO, NO_2, and SO_2 due to boundary-layer compression and intensified combustion; pre-monsoon promoted O_3 and HCHO build-up under high solar irradiance; and monsoon months recorded the lowest pollutant loadings, confirming wet scavenging efficiency and cloud-mediated radiation attenuation. Spatial mapping revealed persistent hotspots over southern power plant clusters, while northern and peripheral zones showed lower concentrations, reflecting the influence of regional land use on pollutant dispersion. Mann–Kendall analysis indicated stable but incrementally increasing tendencies for CO, SO_2, and O_3, with a slight NO_2 decline suggesting partial emission control effectiveness [67,68]. Spearman correlation confirmed synchronous combustion origin (CO–NO_2 ρ = 0.78; NO_2–SO_2 ρ = 0.72) and strong radiative control of secondary chemistry (Solar–O_3 ρ = 0.75; Solar–HCHO ρ = 0.61), with cloud-induced suppression further modulating oxidative capacity. Effective air quality improvement requires integrated emission–radiation–dispersion management. Priority interventions include FGD deployment, low-NO_x burner retrofits, NO_x–VOC precursor regulation for photochemical ozone control, and the establishment of vegetative buffer in industrial peripheries [28,69]. The satellite-based framework demonstrated here is scalable across India's industrial energy corridors, offering a replicable monitoring blueprint for regions lacking dense ground-based instrumentation and supporting objectives of India's National Clean Air Programme.

Author Contribution

Conceptualization, B.K. and N.C.G.; methodology, B.K.; software, B.K.; formal analysis, B.K.; data curation, B.K.; writing original draft preparation, B.K.; writing review and editing, N.C.G.; supervision, N.C.G. Both authors read and approved the final manuscript.

Funding

No funding was obtained for this study.

Institutional Review Board Statement

Not applicable. This study did not involve human participants, human-derived data, or animal subjects.

Informed Consent Statement

Not applicable. This study is based entirely on publicly available satellite data and does not involve human subjects.

Data Availability Statement

Sentinel-5P TROPOMI Level-3 data are freely available through the Google Earth Engine public data catalogue (https://developers.google.com/earth-engine/datasets). Surface shortwave downward irradiance data are accessible via the NASA POWER portal (https://power.larc.nasa.gov). Administrative boundary polygons were obtained from the Global Administrative Database (https://gadm.org). No proprietary datasets were used in this study.

Conflicts of interest

The authors declare no conflict of interest or personal relationships that could have appeared to influence the research reported in this paper.

AI Use Statement

During the preparation of this manuscript, the authors used AI tools solely for language refinement and grammar checking. No AI tools were used for data analysis, data interpretation, figure generation, or the generation of scientific content. All outputs were critically reviewed, verified, and edited by the authors. The authors take full responsibility for the integrity and accuracy of the work presented.

References

[1] WHO, 2021. WHO Global Air Quality Guidelines: Particulate Matter ($PM_{2.5}$ and PM_{10}), Ozone, NO_2, SO_2 & CO. World Health Organization: Geneva, Switzerland. Available from: https://www.who.int/publications/i/item/9789240034228

[2] Guttikunda, S.M., Goel, R., Pant, P., 2019. Nature of air pollution, emission sources, and management in Indian cities. Atmospheric Environment. 95, 501–510.

[3] Granier, C., Bessagnet, B., Bond, T., et al., 2011. Evolution of anthropogenic and biomass burning emissions of air pollutants at global and regional scales during the 1980–2010 period. Climatic change. 109(1), 163.

[4] Ambikan, A.T., Dasgupta, S., Dhar, R., et al., 2025. Exposure to Household Biomass Burning and Coal-Fired Power Plant Emissions Exacerbates Biological Aging in Females-A Case-Control Study. DOI: https://dx.doi.org/10.2139/ssrn.5738405

[5] Aher, S.B., Dobhal, R.S., Awasthi, 2014. Spatial and temporal variations of SO_2, NOx, PM_{10} and TSPM concentration in ambient air of Jalna City, India. International Journal of Agriculture, Environment and Biotechnology. 7(3), 571–579. DOI: https://doi.org/10.5958/2230-732X.2014.01362.X

[6] Aher, S.B., Nandi, S., Ramesh, G., et al., 2022. Effects of COVID-19 lockdown on ambient air pollution in Madhya Pradesh, India. International Journal of Environmental Studies. 79(3), 401–416. DOI: https://doi.org/10.1080/00207233.2021.1929412

[7] Goto, D., Yashiro, H., Yamashita, Y., et al., 2026. Assessment of the impacts of anthropogenic ozone precursors on domestic and transboundary ozone concentrations using a high-resolution global chemistry model. Progress in Earth and Planetary Sciences. 13, 3. DOI: https://doi.org/10.1186/s40645-025-00791-7

[8] Peters, A., Pope, C.M., 2002. Cardiopulmonary mortality and air pollution. The Lancet. 360(9341), 1184–1185.

[9] Jaganathan, S., Stafoggia, M., Rajiva, A., et al., 2024. Estimating the effect of annual $PM_{2.5}$ exposure on mortality in India: A difference-in-differences approach. The Lancet Planetary Health. 8, e987–e996.

[10] Nguyen, N.H., Turner, A.J., Yin, Y., et al., 2020. Effects of Chemical Feedbacks on Decadal Methane Emissions Estimates. Geophysical Research Letters. 47(7), e2019GL085706. DOI: https://doi.org/10.1029/2019GL085706

[11] Ojha, N., Naja, M., Singh, K. P., et al., 2012. Variabilities in ozone at a semi-urban site in the Indo-Gangetic Plain region: Association with the meteorology and regional processes. Journal of Geophysical Research: Atmospheres. 117(D20). DOI: https://doi.org/10.1029/2012JD017716

[12] Zhang, H., Wu, S., Huang, Y., 2014. Effects of stratospheric ozone recovery on photochemistry and ozone air quality in the troposphere. Atmospheric Chemistry and Physics. 14(8), 4079–4086.

[13] Jethva, H., Torres, O., Ahn, C., 2014. Global assessment of OMI aerosol single-scattering albedo using ground-based AERONET inversion. Journal of Geophysical Research: Atmospheres. 119(14), 9020–9040.

[14] Fadnavis, S., Mahajan, A.M., Choudhury, A.D., et al., 2020. Atmospheric aerosols and trace gases. In: Krishnan, R., Sanjay, J., Gnanaseelan, C., et al. (Eds.). Assessment of Climate Change over the Indian Region: A Report of the Ministry of Earth Sciences (MoES), Government of India. Springer Singapore: Singapore. pp. 93–116.

[15] Monks, P.S., Archibald, A.T., Colette, A., et al., 2015. Tropospheric ozone and its precursors from the urban to the global scale from air quality to short-lived climate forcer. Atmospheric Chemistry and Physics. 15(15), 8889–8973.

[16] Kondratyev, K.Y., Varotsos, C.A., 1996. Global total ozone dynamics: Impact on surface solar ultraviolet radiation variability and ecosystems Part I: Global ozone dynamics and environmental safety (*ESPR 3/96*) Part II: Dynamics of atmospheric chemical composition: The role of remote sensing (*ESPR 4/96*). Environmental Science and Pollution Research. 3(4), 153–157.

[17] Anderson, D.C., Duncan, B.N., Fiore, A.M., et al., 2021. Spatial and temporal variability in the hydroxyl (OH) radical: Understanding the role of large-scale climate features and their influence on OH through its dynamical and photochemical drivers. Atmospheric Chemistry and Physics. 21(8), 6481–6508.

[18] Musiolková, M., Huszár, P.H., Navrátil, M., et al., 2021. Impact of season, cloud cover, and air pollution on different spectral regions of ultraviolet and visible incident solar radiation at the surface. Quarterly Journal of the Royal Meteorological Society. 147(738), 2834–2849.

[19] Plocoste, T., Calif, R., Euphrasie-Clotilde, L., et al., 2020. Investigation of local correlations between particulate matter (PM_{10}) and air temperature in the Caribbean basin using Ensemble Empirical Mode Decomposition. Atmospheric Pollution Research. 11(10), 1692–1704.

[20] Kumar, P., Choudhary, A., Joshi, P.K., et al., 2025. Machine learning models for estimating criteria pollutants and health risk-based air quality indices over Eastern Coast coal mine complex belts. Frontiers in Environmental Science. 13, 1589991.

[21] Singh, A.K., Shukla, S.K., 2025. Assessing Air Pollution Tolerance, Photosynthetic Pigmentation, and Dust

Capturing Capacity of Roadside Trees in the Mining Region. Journal of Sustainable Forestry. 44(7), 572–598.
[22] CPCB, 2021. Comprehensive Environmental Pollution Index (CEPI) Report: Critically Polluted Industrial Clusters. Ministry of Environment, Forest & Climate Change: New Delhi, India.
[23] Huang, H., Chen, T.K., Kamalanathan, S., et al., 2025. Spatiotemporal Analysis of Urban Air Pollution Dynamics: Linking Emission Sources, Meteorological Influences, and Public Health Risks Through Long-Term Monitoring. Applied Ecology and Environmental Research. 23(6), 10559–10589.
[24] Yadav, A.K., Shirin, S., Emmanouil, C., et al., 2022. Effect of seasonal and meteorological variability of air pollution in Singrauli coalfield. Aerosol Science and Engineering. 6(1), 61–70.
[25] Srivastava, A., Thakur, A.K., Garg, R.D., et al., 2025. Spatiotemporal analysis of NO_2 trends over major air pollution hotspots in India using Sentinel-5P. Journal of Earth System Science. 134(3), 172.
[26] Srivastava, A., Thakur, A.K., Garg, R.M., et al., 2026. A Comprehensive Assessment of Spatiotemporal Dynamics of Urban NO_2 using Sentinel-5P with Evaluation of the Predictive Capability of Sentinel-2 for Pollution Estimation. Water, Air, & Soil Pollution. 237(6), 382.
[27] MoEFCC, 2020. National Clean Air Programme (NCAP). Ministry of Environment, Forest & Climate Change, Government of India:New Delhi, India.
[28] Kumar, R., Yadav, S., Verma, A., et al., 2026. Metal pollution in roadside dust of Singrauli power belt in central India and associated human health risk. Environmental Monitoring and Assessment. 198(2), 151.
[29] Bose, R.K., Leitmann, J., 1996. Environmental profile of the Singrauli region. Cities. 13(2), 71–77.
[30] Roy, D., Singh, G., 2014. Source apportionment of particulate matter (PM_{10}) in an integrated coal mining complex of Jharia coalfield, Eastern India: A review. International Journal of Engineering Research and Applications. 4(4), 97–113.
[31] Behera, S., Kannemadugu, H.B.S., Divy, K.G., et al., 2025. Satellite-based monitoring of NO_2 concentrations over thermal power plants around Delhi and assessing their role in Delhi air pollution. International Journal of Remote Sensing. DOI: https://doi.org/10.1080/01431161.2025.2559424
[32] Kayes, I., Shahriar, S.A., Hasan, M., et al., 2019. The relationships between meteorological parameters and air pollutants in an urban environment. Global Journal of Environmental Science and Management. 5(3), 265–278.
[33] Nagpure, B.R., Gurjar, A.S., Kumar, P., et al., 2010. Pollutant emissions from road vehicles in megacity Kolkata, India: Past and present trends. Indian Journal of Air Pollution Control. 10(2), 18–30.
[34] Ialongo, I., Virta, H., Eskes, H., et al., 2020. Comparison of TROPOMI/Sentinel-5 Precursor NO_2 observations with ground-based measurements in Helsinki. Atmospheric Measurement Techniques. 13(1), 205–218.
[35] Wu, S., Huang, B., Wang, J., et al., 2021. Spatiotemporal mapping and assessment of daily ground NO_2 concentrations in China using high-resolution TROPOMI retrievals. Environmental Pollution. 273, 116456.
[36] ESA, 2024. Copernicus Sentinel-5P TROPOMI Level-2 Data Products. Available from: https://sentinels.copernicus.eu/data-products/-/asset_publisher/fp37fc19FN8F/content/tropomi-level-2-tropospheric-ozone (cited 10 April 2026).
[37] Gorelick, N., Hancher, M., Dixon, M., et al., 2017. Google Earth Engine: Planetary-scale geospatial analysis for everyone. Remote Sensing of Environment. 202, 18–27.
[38] Mustafa, A.A., Shokr, M.S., Alharbi, T., et al., 2025. Integration of Google Earth Engine and Aggregated Air Quality Index for Monitoring and Mapping the Spatio-Temporal Air Quality to Improve Environmental Sustainability in Arid Regions. Sustainability. 17(8), 3450.
[39] Gawhane, R.D., Nikam, M., Karri, D., et al., 2026. Interplay between anthropogenic emissions, monsoon circulation, and trace metal deposition in rainwater over a rapidly urbanizing region of southwestern India. Available from: https://www.researchgate.net/publication/398778575_Interplay_between_anthropogenic_emissions_monsoon_circulation_and_trace_metal_deposition_in_rainwater_over_a_rapidly_urbanizing_region_of_southwestern_India (cited 10 April 2026).
[40] Saw, G.K., Dey, S., Kaushal, H., et al., 2021. Tracking NO_2 emission from thermal power plants in North India using TROPOMI data. Atmospheric Environment. 259, 118514.
[41] Levelt, P.F., Stein Zweers, D.C., Aben, I., et al., 2022. Air quality impacts of COVID-19 lockdown measures detected from space using high spatial resolution observations of multiple trace gases from Sentinel-5P/TROPOMI. Atmospheric Chemistry and Physics Discussions. 22(5), 10319–10351.
[42] Zeb, N., Khokhar, M.F., Pozzer, A., et al., 2019. Exploring the temporal trends and seasonal behaviour of tropospheric trace gases over Pakistan by exploiting satellite observations. Atmospheric Environment. 198, 279–290.
[43] Aher, S.B., Raj, D., Nandi, S., 2025. Air pollution spikes and health risks resulting from wheat crop residue burning in central India. Journal of Health Science Research. 10(2), 43–53. DOI: https://doi.org/10.25259/jhsr_11_2025
[44] Aher, S.B., Raj, D., Saroj, P., et al., 2026. Short-term $PM_{2.5}$ concentration increases outpace PM_{10} during Diwali in Madhya Pradesh, Central India. Water, Air, & Soil Pollution. 237, 777. DOI: https://doi.org/10.1007/

s11270-026-09457-6

[45] Census of India, 2011. District Census Handbook: Singrauli. Office of the Registrar General & Census Commissioner, India: New Delhi, India.

[46] India Meteorological Department, 2024. Climatological Summaries of States Series—No. 27, IMD Report No. "MoES/IMD/CLI-REP(M.P.)/01(2024)/19": Climate of Madhya Pradesh. India Meteorological Department: Pune, India.

[47] NGT, 2020. National Green Tribunal Order on Critically Polluted Areas. National Green Tribunal, Government of India: New Delhi, India.

[48] Wang, W., Li, X., Cheng, Y., et al., 2024. Ozone pollution mitigation strategy informed by long-term trends of atmospheric oxidation capacity. Nature Geoscience. 17(1), 20–25.

[49] Deng, W., Wang, L., Huang, J., et al., 2026. Photochemical ozone formation-oriented VOC source apportionment and health economic burdens in Pearl River Delta. npj Clean Air. 2(1), 16.

[50] Aher, S.M., Trushna, T., Raj, D., et al., 2025. Impact of crop residue burning on ambient $PM_{2.5}$ and PM_{10} dynamics in Jharkheda Village, Central India. CLEAN—Soil, Air, Water. 53(11), e70065. DOI: https://doi.org/10.1002/clen.70065

[51] Tanwar, N., Aher, S.B., Raj, D., et al., 2025. Investigating the Impact of Meteorological Parameters on $PM_{2.5}$ Concentrations and Air Quality Index Using Regression Analysis. Journal of Atmospheric Science Research. 8(4), 10–18.

[52] Rahman, M.M., Kamruzzaman, M., Faridatul, M.I., et al., 2025. Spatiotemporal dynamics of urban air pollution in Dhaka City (2020–2024) using time-series sentinel-5P satellite images and Google earth engine (GEE). Environments. 12(8), 274.

[53] Ahmed, M.F., Rana, B., Halder, B., et al., 2025. Assessing atmospheric pollution in Asian major cities through sentinel-5p and google earth engine: A remote sensing approach. Theoretical and Applied Climatology. 156(9), 458.

[54] Halder, B., Rana, B., Ahmed, M.F., et al., 2026. Spatiotemporal air quality monitoring using Sentinel 5P in the arid region for environmental sustainability. Air Quality, Atmosphere & Health. 19(2), 23.

[55] Mondal, S., Singh, G., Jain, M.K., 2020. Spatio-temporal variation of air pollutants around the coal mining areas of Jharia Coalfield, India. Environmental Monitoring and Assessment. 192(6), 405.

[56] Pandey, B., Agrawal, M., Singh, S., 2014. Assessment of air pollution around coal mining area: Emphasizing on spatial distributions, seasonal variations and heavy metals, using cluster and principal component analysis. Atmospheric Pollution Research. 5(1), 79–86.

[57] Pathak, B., Bhuyan, P.K., 2022. Characteristics of atmospheric pollutants over the northeastern region of India. In: Singh, P.R. (Ed.). Asian Atmospheric Pollution: Sources, Characteristics and Impacts. Elsevier: Amsterdam, The Netherlands. pp. 367–392.

[58] Singh, S., Kumar, R., 2022. Air pollution and its associated impacts on atmosphere and biota health. In: Saxena, P., Shukla, A., Gupta, A.K. (Eds.). Extremes in Atmospheric Processes and Phenomenon: Assessment, Impacts and Mitigation. Springer Nature Singapore: Singapore. pp. 29–58.

[59] Kunchala, R.K., Singh, B.B., Karumuri, R.K., et al., 2022. Understanding the spatiotemporal variability and trends of surface ozone over India. Environmental Science and Pollution Research. 29(4), 6219–6236.

[60] Tripathi, S.N., Pattnaik, A., Dey, S., 2007. Aerosol indirect effect over Indo-Gangetic plain. Atmospheric Environment. 41(33), 7037–7047.

[61] Singh, N., Banerjee, T., Raju, M.P., et al., 2018. Aerosol chemistry, transport, and climatic implications during extreme biomass burning emissions over the Indo-Gangetic Plain. Atmospheric Chemistry and Physics. 18(19), 14197–14215.

[62] Li, Z., Lau, W.K.-M., Ramanathan, V., et al., 2016. Aerosol and monsoon climate interactions over Asia. Reviews of Geophysics. 54(4), 866–929.

[63] Haywood, J., 2021. Atmospheric aerosols and their role in climate change. In: Letcher, T.M. (Ed.). Climate Change: Observed Impacts on Planet Earth. Elsevier: Amsterdam, The Netherlands. pp. 645–659.

[64] Sun, J., Veefkind, J.P., Van Velthoven, P., et al., 2018. Quantifying the single-scattering albedo for the January 2017 Chile wildfires from simulations of the OMI absorbing aerosol index. Atmospheric Measurement Techniques. 11(9), 5261–5277.

[65] Kumari, M., Bhattacharya, T., 2023. Controlling Air and Metal Pollution in Industrial Area Singrauli, India: Role. In Springer Proceedings in Earth and Environmental Sciences Sustainable Advanced Technologies for Industrial Pollution Control. Springer Nature Switzerland: Cham, Switzerland. pp. 211–227.

[66] CDSE, 2023. Sentinel-5P: Monitoring our atmosphere. Available from: https://dataspace.copernicus.eu/data-collections/copernicus-sentinel-missions/sentinel-5p (cited 10 April 2026).

[67] Yadav, S.K., Kompalli, S.K., Gurjar, B.R., et al., 2021. Aerosol number concentrations and new particle formation events over a polluted megacity during the COVID-19 lockdown. Atmospheric Environment. 259, 118526.

[68] Kumar, P., Mann, M., Gupta, N.C., 2019. Regression analysis of aerosol optical properties with long-term MODIS data using forward selection method. Meteorology and Atmospheric Physics. 131(4), 1121–1131.

[69] Sinha, V., Kumar, V., Sarkar, C., 2014. Chemical composition of pre-monsoon air in the Indo-Gangetic Plain measured using a new air quality facility and PTR-MS: High surface ozone and strong influence of biomass burning. Atmospheric Chemistry and Physics. 14(12), 5921–5941.